Rotational Motions of Macromolecules by Single-Molecule Fluorescence Microscopy

STEPHANIE A. ROSENBERG,[†,⊥]
MARGOT E. QUINLAN,[‡,∥]
JOSEPH N. FORKEY,[‡,§] AND
YALE E. GOLDMAN*[,‡]
Pennsylvania Muscle Institute and Department of Physiology, University of Pennsylvania, Philadelphia, Pennsylvania 19104-6083, and Department of Bioengineering, University of Pennsylvania, Philadelphia, Pennsylvania 19104
Received October 4, 2004

ABSTRACT
Several complementary techniques have been developed to determine average orientation, dynamics on multiple time scales, and concerted rotational motions of individual fluorescent probes bound to biological macromolecules. In both protein domains and nucleic acids, tilting and wobble are relevant to their functional mechanisms. Here we briefly review methods to detect angles and rotational motions of single fluorophores and give an example of three-dimensional, total internal reflection, single-molecule fluorescence polarization applied to actin as it is translocated by conventional muscle myosin.

Introduction

Tilting and rotations of molecular domains are crucial motions in the mechanisms of many protein and RNA enzymes.[1−6] The advantages of single-molecule techniques highlighted in this issue, such as measurement of actual distributions rather than averages and identification of reverse kinetic steps and rare events, apply to detecting rotational motions as well. These factors are especially prominent in molecular motor research because the main functional output, conversion of chemical energy into physical translocation, is commonly attributed to tilting of protein domains.[7,8] In dimeric kinesin isoforms, for example, melting and docking of a peptide segment termed the "neck linker" on one head moves the other head forward.[9] In myosin, the light chain region, also termed the "neck" of myosin's head, serves as a lever arm to amplify subnanometer atomic motions near the active site into 5−20 nm translocation of the cargo.[2,8,10] Changes in spatial orientation of these domains are the key structural changes leading to movement. However, quantifying angle changes in ensemble systems can be very difficult. For example, during contraction of muscle fibers, most of the myosin heads are not attached to actin and have a nearly random angular distribution.[11,12] Concerted rotational motions among the small proportion that are attached to actin are therefore difficult to detect against the disordered background.

Single-molecule fluorescence microscopy provides sufficient sensitivity to detect absolute orientation and tilting on the millisecond time scale relevant to the function of biological macromolecules.[13] In a typical experiment, a bright extrinsic fluorophore is inserted into the structure by site-specific labeling. Changes in the orientation of the fluorophore are considered to signal the rotational motions of the protein or nucleic acid domain in addition to relative motions between the probe and the protein. This type of experiment has been applied to several macromolecules such as DNA,[14,15] RNA enzymes,[16] the F_1 ATP synthase,[17] actomyosin,[18−20] and kinesin.[21,22] When the orientation of the probe is known relative to the attached macromolecular domain, the absolute orientation in space can be estimated.[20,21,23] The relative orientation can be preprogrammed into the structure by the placement of the labeling sites[20,21,23] or determined by crystallography, NMR spectroscopy,[24] or molecular dynamics calculations.[25] With the local probe orientation known, the relative angles between several domains or the kinetics of structural changes that relate to other functional steps in the enzymatic cycle can be deduced.

Measurements of tilting motions and rotation in single molecules were reviewed by Ha et al.,[26] Forkey et al.[13] and Peterman et al.[27] for molecular motors. In this Account, we provide some comparative perspective on various methods to determine orientation and rotational mobility of single fluorophores and give an example, determining

Stephanie A. Rosenberg obtained the Bachelor of Science in Physics from Emory University in 2001 and the M.S.E. in Bioengineering from the University of Pennsylvania in 2004. She is currently a staff biologist in the Cardiovascular Diseases Department at Merck & Co. where her primary focus is hypertension.

Dr. Margot E. Quinlan obtained the Bachelor of Arts in Biology from Reed College in 1991 and the Ph.D. in Cell and Molecular Biology from the University of Pennsylvania in 2002. She is currently a Postdoctoral Fellow at the University of California, San Francisco, with Dr. R. Dyche Mullins. She is studying the protein Spire, an actin nucleation factor that plays a role in polarity determination in *Drosophila* oogenesis.

Dr. Joseph N. Forkey obtained the Bachelor of Arts in Physics and Mathematics from Cornell University in 1989 and the Ph.D. in Mechanical and Aerospace Engineering from Princeton University in 1996. He was a Postdoctoral Fellow at the University of Pennsylvania with Professor Yale E. Goldman. Dr. Forkey is currently Chief Scientist at Precision Optics Corporation where his work involves applications of single-molecule detection and development of technologies for efficient construction of opto-mechanical systems and for fabrication of submillimeter optical components and assemblies.

Dr. Yale E. Goldman obtained the Bachelor of Science in Electrical Engineering from Northwestern University in 1969 and the M.D. and Ph.D. in Physiology from the University of Pennsylvania in 1975. He was a Postdoctoral Fellow at University College London with Professor Sir Andrew F. Huxley and Dr. Robert M. Simmons and then joined the faculty at the University of Pennsylvania School of Medicine in 1980. Dr. Goldman is former Bowditch Lecturer of the American Physiological Society, Lamport Lecturer of the University of Washington, Wheeler Lecturer of the Aspen Center for Physics, and past President of the Biophysical Society. He is currently Professor and Director of the Pennsylvania Muscle Institute. His scientific research covers biophysical mechanisms of muscle contraction, molecular motors, and protein synthesis by the ribosome and development of novel methods for these studies, including photolysis of caged molecules, oxygen exchange and dynamic fluorescence polarization in supramolecular systems, single-molecule fluorescence polarization microscopy, and high-speed optical traps.

† Department of Bioengineering.
⊥ Current address: Merck & Co., West Point, PA 19486.
‡ Pennsylvania Muscle Institute and Department of Physiology.
∥ Current address: Department of Cellular and Molecular Pharmacology, University of California, San Francisco, CA 94143-2200.
§ Current address: Precision Optics Corporation, Gardner, MA 01440.

10.1021/ar040137k CCC: $30.25
Published on Web 04/16/2005

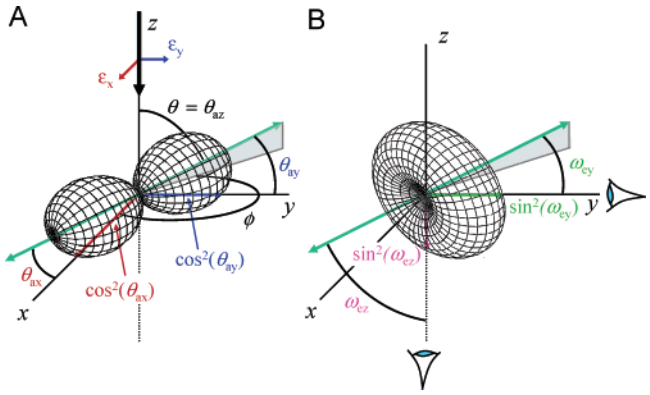

FIGURE 1. Relative probabilities for fluorophore absorption (panel A, $\cos^2 \theta_a$) and collection of its emission (panel B, $\sin^2 \omega_e$). In the microscope coordinate frame (x, y, z), the optical axis is z. For axial illumination (heavy arrow in panel A), ϵ_x and ϵ_y are excitation polarizations. The probe absorption and emission dipole moments (considered to be parallel) in the (x, y, z) frame are defined by θ (axial angle) and ϕ (azimuth, angle between the projection of the dipole onto the $x-y$ plane and the positive x axis). θ_{ax} and θ_{ay} are angles between the probe dipole and detector polarizations along the x- and y-axes. ω_{ey} and ω_{ez} are angles between the probe dipole and detector optical paths in the y- and z-axes.

the angle of rhodamine incorporated in actin and its motions when actin is translocated by myosin.

Detection of Fluorophore Orientation

There are fundamentally three physical properties that enable determination of a fluorophore's spatial orientation: relative absorption of light polarized in various directions, the angular distribution of its emitted photons, and their polarization. The likelihood that a chromophore will absorb a photon is proportional to $\cos^2 \theta_a$, where θ_a is the angle between the photon's polarization (direction of the oscillating electric field) and the absorption dipole moment. In xanthene-derivative dyes, such as rhodamine, the absorption dipole is aligned with the long axis of the conjugated ring system of the chromophore. The shape of the $\cos^2 \theta_a$ function in three dimensions is plotted in Figure 1A, showing that the angular discrimination by this absorption probability is a gradual function of angle. But the amount of fluorescence due to illumination of the fluorophore with light polarized in various directions will discriminate among various angles.[28]

The distribution of paths of photons originating from a dipole emitter is given by $\sin^2 \omega_e$, where ω_e is the angle between the path of the photon and emission dipole moment (Figure 1B). For a detector viewing the fluorophore along a narrow aperture, the likelihood of registering an emitted photon is proportional to $\sin^2 \omega_e$. With wider aperture collecting optics and imaging, the spatial distribution of emission paths can be transformed into a spatial variation in the image.[29] This topic is taken up later in this Account.

When a polarizer is introduced before a narrow-aperture detector, the likelihood of registering the emitted photon is given by $\cos^2 \theta_e$, where θ_e is the angle between the fluorophore emission dipole and the detector polarization. The most common configurations of detectors are a single unpolarized detector[21] or a pair of polarized detectors with the same line of sight but orthogonal polarizations[15,19] We first describe methods based on comparing fluorescence intensities among several excitation or detection polarizations. Various methods using large numerical aperture microscope objectives for generating nonuniform excitation or detection fields, which are scanned across the fluorophore to interrogate its orientation, are considered later in this Account. Combining several of these orientational dependencies of probability for absorption and detection can improve the sensitivity of these techniques.

Single-Molecule Fluorescence Polarization

The orientation of the fluorophore is detected by illuminating the sample with polarized light at various angles and resolving the polarization of the fluorescence emission. Development of microscopes using this property for single molecules evolved in several laboratories. In an early measurement of single-molecule angles in a functioning biological sample, Sase et al.[18] generated epi-illumination excitation using light circularly polarized in the plane of the microscope slide ($x-y$ plane). The components of fluorescence emission polarized along the two orthogonal axes in the same plane were projected separately onto two regions of a video camera detector chip. This setup was used to monitor actin filament rotation about its axis similar to the data presented later in this Account. Warshaw et al.[19] used similar optical polarizations in a confocal microscope to detect rotational motions of the regulatory light chains when myosin attached to actin. With this optical arrangement, the ratio of intensities between the two detectors, corrected for differences in their sensitivity, gives an intensity-independent signal, sensitive to the angle (ϕ) of the projection of the emission dipole onto the $x-y$ plane (Figure 1A). At fluorophore angles giving $\phi = 45°$ or $-45°$, the two recorded intensities are equal, and angular discrimination away from 45° or −45° depends on differences between the two intensities. For a given average angle, rotational mobility of the probe or macromolecule causes the two recorded signals to become more equal, so the degree of mobility cannot be unambiguously discriminated from the mean angle. This arrangement does not provide information regarding the fluorophore angle (θ) relative to the optical axis, because both the exciting and detection polarizations are in the $x-y$ plane. Symmetries in the system prevent angles ϕ and $-\phi$ being distinguished.

This type of ambiguity in ϕ was avoided for studies of DNA motions,[14,15] the mitochondrial F_1 ATP synthase,[17,30] and kinesin[21,22] by illuminating the sample with polarized excitation at multiple angles. In these experiments, the extent of mobility of the sample could be discriminated from the average angle because the ratio of fluorescence intensity when the excitation is aligned with the fluorescent probe to that when excitation is perpendicular to it

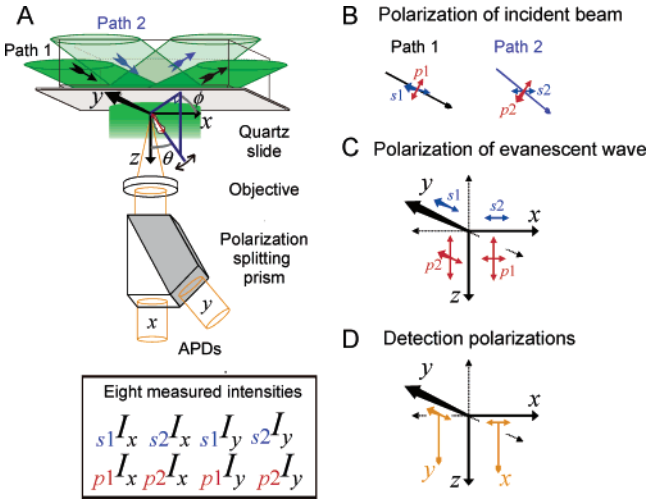

FIGURE 2. Experimental setup for three-dimensional single-molecule fluorescence polarization. Panel A illustrates combining illumination along all three microscope coordinate axes with *x*- and *y*-polarized detection. The input laser is projected along two paths (path 1, scattering plane parallel to the diagram, and path 2, scattering plane perpendicular to the diagram) onto the sample chamber at a high angle relative to *z*, creating an evanescent wave at the slide/sample interface. A bright water-immersion objective, polarization splitting prism, and two avalanche photodiodes (APDs) collect the *x*-polarized and *y*-polarized fluorescence emission. In panel B, with incident p-polarization, the oscillating electric field of the laser beam is parallel to the scattering plane. With s-polarization the $\bar{\mathbf{E}}$-field is perpendicular to the scattering plane. The single-headed arrows show the indicent paths. Panel C illustrates the expected polarizations of the evanescent wave for the four combinations of optical path and polarization. Panel D illustrates the detection polarizations parallel to the *x*- and *y*-axes. The downwardly directed arrows show the emission direction to the detectors.

depends on the mobility. Again, the axial angle θ is not determined with this arrangement.

We built a setup that provides sensitive discrimination of both θ and ϕ, as well as mobility, by combining illumination along all three coordinate axes with *x*- and *y*-polarized detection (Figure 2).[20,31] Angular ambiguities between θ and $180° - \theta$, as well as between ϕ and $-\phi$, are not addressed in this instrument, but potential routes toward breaking these symmetries are described below.

This instrument uses Pockel cells to rapidly modulate the path and polarization of a laser beam that forms an evanescent wave at the interface between the microscope slide and the aqueous sample medium. The laser is projected onto the sample chamber at a shallow angle leading to total internal reflection (Figure 2). Path 1 excitation is in the plane of the diagram; path 2 is perpendicular to the diagram. A scattering plane is defined as the plane containing the incident and reflected beams; with p-polarized excitation, the oscillating electric field of the incident beam is parallel to the scattering plane; with s-polarized excitation, the $\bar{\mathbf{E}}$-field is perpendicular to the scattering plane. Figure 2 shows the expected polarization of the evanescent wave for four combinations of optical path and polarization. The s-polarized excitation beams produce *y*-polarized (path 1) and *x*-polarized (path 2) evanescent waves. The p-polarized excitation beams produce strong *z*-polarized evanescent waves with small (5−10% intensity) components along the *x* (path 1) and *y* (path 2) directions.[32] All three orthogonal directions of the laboratory coordinate frame are represented in these four combinations of path and polarization. In a typical experiment on molecular motors, cycles of the four combinations are completed every 40 ms by alternating the voltages on the Pockel cells. A bright water-immersion objective, a polarizing prism, and two avalanche photodiodes (APDs) collect the *x*-polarized and *y*-polarized fluorescence emission. The counts from the two APDs during each of the four combinations of input path and polarization are binned into eight traces, $_{s1}I_x$, $_{s1}I_y$, $_{p1}I_x$, $_{p1}I_y$, $_{s2}I_x$, $_{s2}I_y$, $_{p2}I_x$, and $_{p2}I_y$, that contain the orientation information with 40 ms time resolution. The raw photocount intensities are corrected for different intensities of the illuminating directions and polarizations, differential detector sensitivity, the longitudinal components of the evanescent wave,[32] and mixing of the *x*- and *y*-polarization emissions by the high-aperture objective.[33] Corrected intensities are then fitted by a model of the probe fluorescence emission, including collinear absorption and emission diploes (for rhodamine).[34,35] The model describes polarized fluorescence as a function of the dipole mean angle defined by θ and ϕ, limited rotational mobility of the probe on the subnanosecond time scale, δ_f, and separately on the microsecond time scale, δ_s, and background intensity measured after photobleaching. Snapshots of the four parameters, θ, ϕ, δ_f, and δ_s, are estimated every 40 ms. A qualitative explanation of the effects on the polarized fluorescence signals of mobility on the two time scales is given in the next section. With square-wave voltages applied, the polarization switches very rapidly (2 μs with the present electronics and ammonium dihydrogen phosphate Pockel cells, which do not exhibit piezoelectric resonance), so much faster excitation cycling and time resolution are feasible at higher illumination intensity.

In the single-molecule fluorescence polarization (SMFP) experiments discussed below, a few hundred photocounts per polarization per 10 ms time gate were recorded. Under these conditions, typical standard deviations on angle measurements from the same static molecule, a measure of the angular precision, were roughly 5°−15°. The main source of this uncertainty is photon shot noise.[31] Shorter time gates would lead to enhanced time resolution at the expense of poorer angular precision due to the associated reduction in number of photons per gate. The reduced photon count rate can be partially mitigated by increasing the excitation power. A significant enhancement of the temporal resolution can be obtained without a sacrifice in angular precision, but with a shorter recording time before the probe photobleaches. Increasing the excitation intensity is ultimately limited by saturation of the fluorophore. For rhodamine, the best time resolution attainable for SMFP with ∼5°−15° angular precision would be approximately 100 μs.

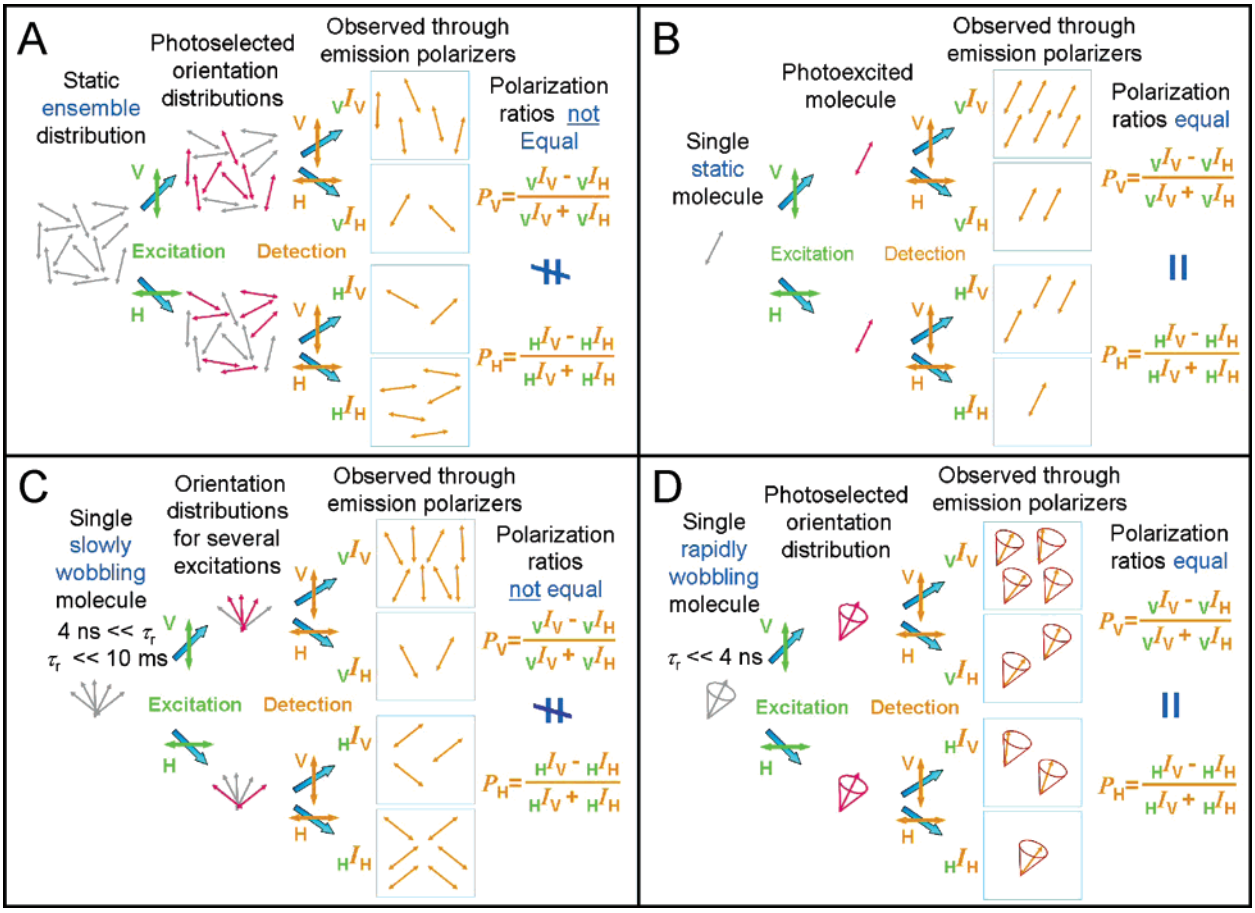

FIGURE 3. Effect of fluorophore rotational mobility on emission polarized fluorescence ratios: (A) when an ensemble of static probes with random orientations is excited at vertical and horizontal polarizations and the fluorescence is detected through vertical and horizontal polarizers, photoselection causes unequal emission polarization ratios ($P_V \neq P_H$); (B) for a single static molecule, once it is excited, the orientation of the illumination is irrelevant to its emission, and emission polarization ratios are equal ($P_V = P_H$); (C) if the single molecule wobbles with rotational correlation time, τ_r, much greater than the fluorescence lifetime, τ_f, but much smaller than the measurement time, τ_c, then $P_V \neq P_H$, as in the ensemble case; (D) if the probe motion is much faster, $\tau_r \ll \tau_f$, then P_V and P_H are equal but smaller than in panel B.

Time Scales Detectable in Single-Molecule Fluorescence Polarization Experiments

In conventional ensemble fluorescence polarization experiments, the effects of mobility of the probe or target macromolecule depend on the time scale of recording. In a nanosecond time-resolved experiment, deviations of the absorption and emission dipole moments from collinearity and rotational motions within the dead time of the instrument control the zero-time anisotropy. Rotational motions on the time scale near the fluorescence excited-state lifetime (τ_f) are directly resolved in the anisotropy decay.[28] Rotational motions much slower than τ_f are not resolved. In steady-state measurements of average anisotropy, the subnanosecond motions and those in the range of τ_f are averaged together. If the experimental sample has intrinsic order, such as a cytoskeletal filament or an ordered stack of membranes, the axial angular distribution relative to the symmetry axis is detectable in addition to the extent of very rapid motion.[36] In single-molecule FP, the average angle of the probe under interrogation is measured, but surprisingly, two other time scales of motion affect the polarized fluorescence intensities in different ways and are therefore subject to estimation. Thus more dynamic information about the probe is accessible in the static (or snapshot) single-molecule case than for the ensemble.

Figure 3 shows qualitatively why this behavior applies. First, consider an ensemble of probes having random orientations but being completely immovable on the time scale of the measurement. Illumination with vertical or horizontal light in the fluorophore absorption band will tend to excite molecules oriented near the direction of the exciting light polarization (Figure 3A). This process, termed photoselection, is caused by the $\cos^2 \theta_a$ absorption probability described earlier. Intensity viewed through a vertical analyzing polarizer will be more intense for vertical illumination than for horizontal illumination and *vice versa* for intensity viewed through a horizontal polarizer. Polarization ratios using vertical excitation, such as $({}_VI_V/{}_VI_H)$ or $P_V = ({}_VI_V - {}_VI_H)/({}_VI_V + {}_VI_H)$, will be different from ratios using horizontal excitation, such as $({}_HI_V/{}_HI_H)$ or $P_H = ({}_HI_V - {}_HI_H)/({}_HI_V + {}_HI_H)$, where the leading subscript is the polarization of the excitation and the trailing subscript is the polarization of the analyzer. In the case shown in Figure 3A, $({}_VI_V/{}_VI_H) \neq ({}_HI_V/{}_HI_H)$ and $P_V = -P_H$, the inequali-

ties being caused by the optical photoselection and subsequent immobility.

For a single static molecule, the situation is quite different (Figure 3B). Vertical and horizontal illumination may have different probabilities for excitation, but once the molecule is excited, the orientation of the illumination does not matter. The excited molecule is exactly the same whether the illumination was vertical or horizontal. Then $({}_{V}I_{V}/{}_{V}I_{H})$ exactly equals $({}_{H}I_{V}/{}_{H}I_{H})$ and $P_V = P_H$. If, on the other hand, the single molecule has wobbling mobility on the time scale $\gg\tau_f$ but faster than the measurement time (τ_c, e.g., 10 ms in the setup described in the previous section), it will be excited several times during a measurement, but more often when it is aligned with the excitation than when it is perpendicular (Figure 3C). In this series of excitation−emission events, a photoselection takes place very similar to that in the static ensemble case of panel A and $({}_{V}I_{V}/{}_{V}I_{H}) \neq ({}_{H}I_{V}/{}_{H}I_{H})$ and $P_V \neq P_H$. The inequalities here are due to the mobility $\tau_f \ll \tau_r \ll \tau_c$, where τ_r is the rotational correlation time of the actual probe motion.

If the probe motion is much faster, $\tau_r \ll \tau_f$, then the effect on the polarization ratios is different again (Figure 3D). The average time between excitation and emission of a fluorescence photon is τ_f . Regardless of the orientation of the probe at the moment of excitation, the probe will visit the entire distribution of angles (within its limited range of rapid wobbling), on average, before it emits the fluorescent photon. The emission is again independent of excitation polarization. The equalities $({}_{V}I_{V}/{}_{V}I_{H}) = ({}_{H}I_{V}/{}_{H}I_{H})$ and $P_V = P_H$ again apply, but the numerical values of the ratios themselves are smaller than in the static case because the rapid wobble tends to reduce the difference between ${}_{V}I_{V}$ and ${}_{V}I_{H}$ and between ${}_{H}I_{V}$ and ${}_{H}I_{H}$. In the limit where the rapid wobble is completely unrestricted, ${}_{V}I_{V} = {}_{V}I_{H} = {}_{H}I_{V} = {}_{H}I_{H}$ and $P_V = P_H = 0$.

These qualitative arguments show how two separate time scales of rotational motion affect single-molecule polarized fluorescence intensities differently. They can be discriminated from each other and from the mean angle if they are both present. Another way of describing this situation is to consider the general relationship between rotational mobility and polarized fluorescence intensity, ${}_{\epsilon}I_{\alpha}$:

$$ {}_{\epsilon}I_{\alpha} = K\int_0^{\infty}\int\int \rho(\theta_a,\phi_a,\theta_e,\phi_e,t)(1/\tau)\, e^{-(t/\tau)}\, P_a(\theta_a,\phi_a,\hat{\epsilon})P_e(\theta_e,\phi_e,\hat{\alpha})\, d\Omega_a\, d\Omega_e\, dt $$

where $\hat{\epsilon}$ is the orientation of the exciting electric field, $\hat{\alpha}$ is the orientation of the analyzer, K is an intensity scaling coefficient, $\rho(\theta_a,\phi_a,\theta_e,\phi_e,t)$ is a correlation function that describes the probability density of finding the absorption dipole at orientation (θ_a,ϕ_a) and the emission dipole at orientation (θ_e,ϕ_e) some time t later. $P_a(\theta_a,\phi_a,\hat{\epsilon})$ is the relative probability of absorbing a photon, given absorption dipole orientation (θ_a,ϕ_a) and electric field polarization $\hat{\epsilon}$. $P_e(\theta_e,\phi_e,\hat{\alpha})$ is the relative probability of detecting an emitted photon, given emission dipole (θ_e,ϕ_e) and analyzer at $\hat{\alpha}$. The factor $(1/\tau_f)\, e^{-(t/\tau_f)}$ is a weighting function that expresses the normalized probability of emitting a photon at time t after excitation, assuming the fluorescence lifetime, τ_f . The integrations are taken over all possible orientations of absorption and emission dipole and over time. $d\Omega_a = \sin\theta_a\, d\theta_a\, d\phi_a$; $d\Omega_e = \sin\theta_e\, d\theta_e\, d\phi_e$ (see also refs 15 and 37).

In the integral above for the case of fast wobble, $\rho(\theta_a,\phi_a,\theta_e,\phi_e,t)$ can be written as the product of two time-independent distribution functions, $\rho_{fa}(\theta_a,\phi_a)$ and $\rho_{fe}(\theta_e,\phi_e)$, which describe the independent probabilities of finding the absorption and emission dipoles in particular orientations. Then the terms representing absorption probabilities can be integrated separately from those containing emission probabilities. For slow wobble, the emission orientation is not independent of the orientation at the moment of absorption and the integral is not separable.

Although these points have been made before,[13,15,20,26] the discussion above and Figure 3 are intended to provide intuition into how the time scales of motion influence the polarized fluorescence in different ways. In practice, analytical equations taking these factors into account, as well as imperfections of the microscope symmetries, are fitted to the eight polarized fluorescence intensity traces to determine K, θ, ϕ, and δ_f and δ_s, the latter two parameters specifying the extent of wobble on the fast and slow time scales. These equations are over-determined (five adjustable parameters, eight intensity samples per time point), allowing a test of goodness of fit and appropriateness of the quantitative description.

Actin

As an example of the use of fluorescence polarization to determine the orientation and mobility of single molecules, we use actin filaments very sparsely labeled with acetamidotetramethyl rhodamine at the reactive residue, Cys[374].[31] Actin and myosin II were purified from rabbit skeletal muscle. The actin was polymerized using 0.3% rhodamine-labeled actin and stabilized with Alexa-647 phalloidin (Molecular Probes, Inc.). Flow chambers were coated with poly-L-lysine to attach full-length myosin, followed by inhibition with BSA, blocking of damaged myosins with short lengths of unlabeled actin, an ATP-containing motility buffer (see Figure 4 legend), and finally, the labeled actin. The observation solution contained either zero or 25 μM ATP and either a deoxygenating cocktail of glucose, glucose oxidase, catalase (GLOXY), and 10 mM DTT or 50 mM DTT in the absence of deoxygenating enzymes. Video images of the rhodamine and Alexa fluorescence were used to locate individual rhodamine fluorophores within actin filaments. Once a particular fluorophore was selected and moved automatically to the stage position conjugate to the recording avalanche photodiodes,[31] sets of the eight polarized fluorescence intensities described above were collected at 40 ms per set for 10 s.

Polarized fluorescence intensities acquired from a typical stationary actin monomer (at 0 ATP, 50 mM DTT) are essentially flat until they bleach simultaneously to the

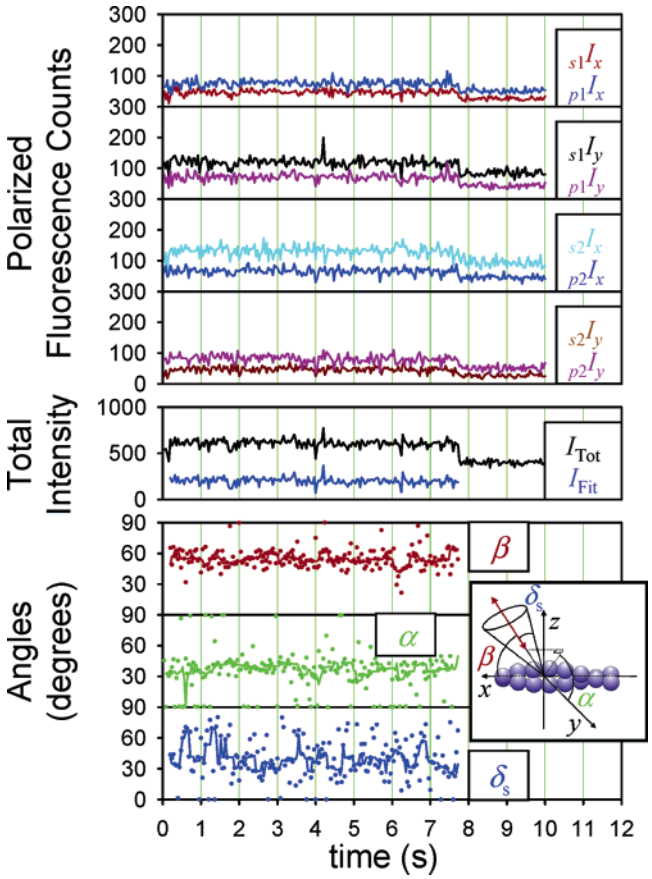

FIGURE 4. Typical single-molecule polarized fluorescence data for a stationary actin filament, sparsely labeled with rhodamine at Cys[374]. Alternation of excitation pathways (1 and 2) and excitation polarizations (s and p) and simultaneous collection with two detector polarizations (*x* and *y*) produces eight measurements every 40 ms. Detected photon counts in each 10 ms interval are plotted as eight polarized fluorescence intensities. A weighted, orientation-independent sum, I_{Tot}, is plotted in black in panel 5. The eight intensities are fit to determine the orientation β (red), α (green), slow wobble, δ_s (blue), and weighted total fitted intensity minus background, I_{Fit} (blue). The average angles for this molecule are $\beta = 54°$, $\alpha = 37°$, and $\delta_s = 39°$. The intensity levels and angles are constant as expected in actin in the absence of ATP. The assay buffer contained 25 mM KCl, 20 mM *N*-2-hydroxyethylpiperazine-*N*′-2-ethanesulfonic acid (Hepes), pH 7.4, 5 mM $MgCl_2$, and 10 mM DTT.

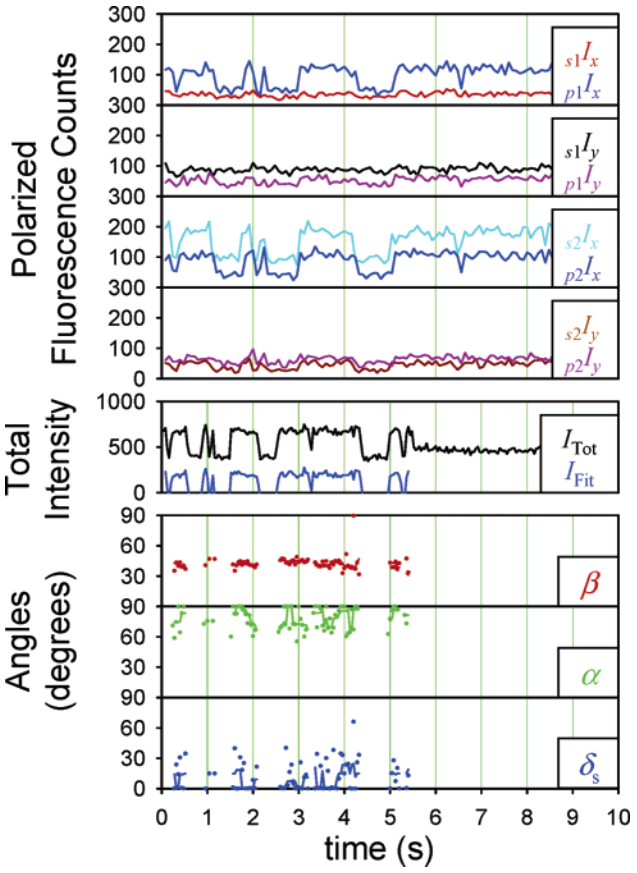

FIGURE 5. Blinking of fluorophore seen when 3 mg/mL glucose, 0.1 mg/mL glucose oxidase, and 0.075 mg/mL catalase are added to the assay buffer. Values of β, α, and δ_s were constant (except for noise) during the "on" intervals suggesting a fixed orientation of the fluoropohore.

background level (Figure 4, upper four panels), indicating that the photons detected above the background come from a single fluorophore. The total fluorescence counts per 40 ms recording interval (200−250) are distributed in a single narrow peak, confirming the single-molecule assignment. A linear combination of the eight intensities that is approximately independent of fluorophore orientation (I_{Tot}, fifth panel) is also constant until the rhodamine bleaches in a single step (at 7.7 s in Figure 4). Laboratory-frame polar angles (θ and ϕ, Figure 2) and the extent of microsecond wobble (δ_s, the half-angle of a cone describing restricted rotational diffusion of the fluorophore on the 4 ns $\ll \tau_r \ll$ 10 ms time scale) were obtained by fitting of analytical equations describing polarized fluorescence intensities to the eight traces.[31] These parameters were converted to angles relative to the axis of the F-actin, which is the natural reference orientation for this system and is stable on the measurement time scale. β is the axial angle of the fluorophore's dipole moment relative to the actin axis, and α is the azimuthal angle around the actin axis (Figure 4, bottom 3 panels). Thus, these angles measure orientation of the individual probe and actin monomer relative to the overall polymeric structure of the filament. Until the bleaching step, all of these angles are approximately constant, except for noise, which is due mainly to the statistics of photon counting.

When the experiment is performed with the GLOXY system added to the motility buffer to decrease oxygen-dependent bleaching, fluorescence intensity traces switch abruptly back and forth between high values and ones near the background level (Figure 5). This repeated blinking of the fluorophore on the ∼1 s time scale abolishes detectable orientation information during the "off" intervals. However, during "on" intervals, the fluorophore maintains an approximately fixed orientation. Similar blinking has been reported previously for rhodamines,[38−40] GFP,[41,42] and other fluorphores.[43,44] The duration of the "off" intervals observed here (∼0.25 s) is probably too long to represent population of the triplet state. Rather, a reversible structural transition or chemical change in the fluorophore, such as ionization or oxidation/reduction, renders it temporarily nonfluorescent. This behavior might be useful in experimental methods that

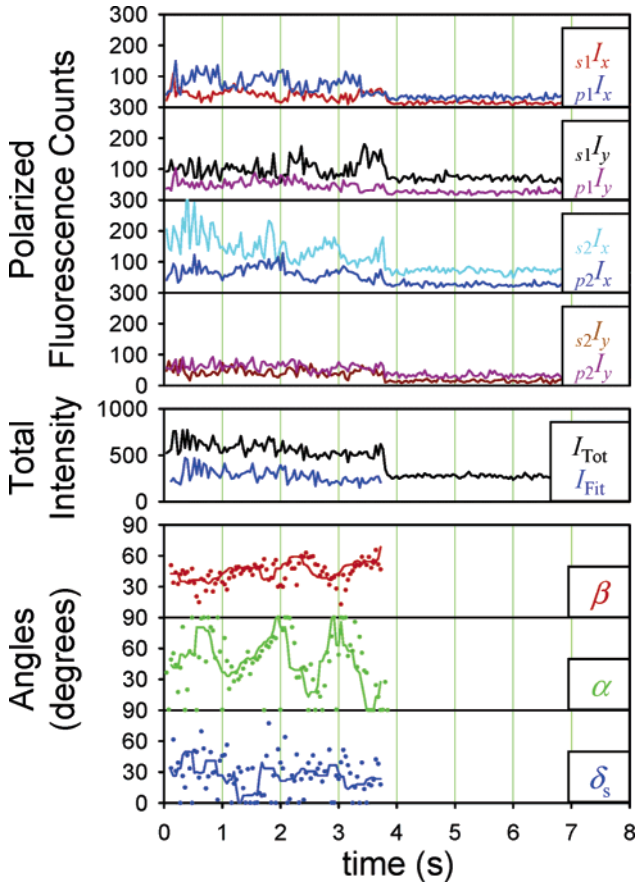

FIGURE 6. Typical single-molecule polarized fluorescence data for an actin filament that is translocated by myosin II in the presence of 25 μM MgATP, 1 mM creatine phosphate, and 1 mg/mL creatine phosphokinase. Values of β and δ_s are roughly constant within each trace, whereas α exhibits a large oscillation. The average angles for this molecule are $\beta = 45°$, $\alpha = 49°$, and $\delta_s = 26°$. The standard deviation of α is 22°.

depend on appearance or disappearance of single-molecule fluorescence, such as nanometer spatial discrimination of two fluorophores by high-resolution imaging with photobleaching (SHRIMP).[45]

When the GLOXY system is replaced with 50 mM DTT, blinking is very rare. The rate of irreversible photobleaching is lower with the GLOXY system present, but using high DTT concentration instead essentially eliminates blinking and allows recording of polarization signals for 1−10 s at illumination levels leading to photocount rates of 5000−7500 s^{-1}.

At 25 μM ATP added to the medium, the actin is translocated by myosin at an average velocity of 0.18 μm/s. Fluorophores are selected that are moving with the actin filaments. During myosin-induced motion, the angles describing the orientation of actin-bound fluorophores exhibit distinctly higher variations of β and α within each temporal trace (Figure 6). Especially noticeable is a roughly sinusoidal pattern of changes in α, indicating that the actin twists about its axis as it moves axially. The microsecond wobble parameter, δ_s, is still relatively constant.

Average values of the actin-frame angles, $\bar{\beta}$, $\bar{\alpha}$, and $\bar{\delta}_s$, using sparsely rhodamine-labeled actin filaments oriented within ±10° of the x-axis were 41° ± 2°, 31° ± 4°, and 31° ± 5° (means among filament averages ± sem, $n = 12$), respectively, at 0 ATP and 51° ± 1°, 44° ± 1°, and 34° ± 1°, respectively, at 25 μM ATP ($n = 79$). The relatively high mobility of actin monomers on the microsecond time scale implies torsional flexibility consistent with spectroscopic and electron microscopic observations.[31] Standard deviations of β, α, and δ during individual traces averaged 4.3°, 10.7°, and 8.4°, respectively, at 0 ATP and 8.8°, 15.6°, and 9.9°, respectively, at 25 μM ATP. These values indicate that, on average, β and especially α vary more in the presence of ATP than in its absence. When the subnanosecond wobble parameter, δ_f, was included as an adjustable parameter in the angular determination, the average values obtained, $\bar{\delta}_f$, were 20° ± 2° at 0 ATP and 24° ± 1° at 25 μM ATP. The other angles, (θ, ϕ, β, α, and δ_s) are essentially the same whether δ_f is made adjustable or not. In most traces, α varied through a much wider angle than β. This behavior is expected for a twisting motion, which would affect α but not β or δ_f. The results suggest that the methodology and analysis enable independent determination of these angles.

From Fourier transforms of the α traces, used to estimate the sinusoidal frequency of the oscillation, and the filament velocities, the pitch of this twisting was calculated to be 0.53 ± 0.07 μm, much longer than the 74 nm pitch of the actin structure. The calculation assumes that two cycles of the observed sinusoidal oscillation of α correspond to one full azimuthal rotation of the actin, because the symmetries in the apparatus described above cause angles α, 180° − α, −α, and −180° + α to produce the same polarized fluorescence intensities. Possible routes to avoid this degeneracy are taken up further below. Some earlier studies also indicated twisting of actin filaments during in vitro motility[18,46,47] but not universally.[48,49] Sase et al.[18] obtained a similar pitch, 1 μm, of actin motion to that obtained here. In that study, though, motions of β could not be distinguished from those of α. Under the present experimental conditions that produce helical motion, myosin exerts an azimuthal force as well as an axial one. This component of force may be very small, however, because the pitch of the motion is large.

Breaking Symmetries in Fluorescence Polarization Experiments

As mentioned, the single-molecule fluorescence polarization microscope in our laboratory was carefully aligned with all polarizers and scattering planes in the x- y- or z-axes. Symmetry about all three axes results in the mean angle measurement having an 8-fold ambiguity. Probes at angles ϕ, 180° − ϕ, −ϕ, and −180° + ϕ all appear identical. Similarly probes at θ and 180° − θ appear identical. Because of the C_2 (180° rotational) symmetry in the interaction between the electromagnetic field and an electrical dipole, it is impossible, with one optical probe, to distinguish orientation (θ,ϕ) from (180° − θ,ϕ − 180°).

The other four angular ambiguities present in measurements using only *x*-, *y*-, and *z*-polarized fields and detectors may be distinguished, in principle, by using alternate or additional orientations of the polarized excitation, emission, or both.

With axial illumination in a confocal or wide-field epi-illumination microscope, intermediate polarization angles, such as 45° and 135° relative to the *x*-axis, result in polarization between the *x*- and *y*-axes, allowing discrimination between angles ϕ and $-\phi$.[14,15,21,22,30] Detector polarizations intermediate between the *x*- and *y*-axes would also remove this ambiguity. In the total internal reflection fluorescence microscopy (TIRFM) arrangement, if the optical path of the exciting light is rotated <90° about the optical axis (e.g., 45°), the scattering plane is between the $x-z$ and $y-z$ planes. The evanescent field generated by s-polarized excitation then generates polarization at the sample between the *x*- and *y*-axes.[17] Molecules having angles ϕ and $-\phi$ have different absorption probabilities under this illumination and thus can be distinguished.

Adding linear optical polarizations between the s- and p-polarizations shown in Figure 2 also enables discrimination of ϕ and $-\phi$. Prummer et al.[50] used a similar method to resolve the three-dimensional orientation of dioctadecyl-tetramethylindocarbocyanine (DiI) fluorophores immobilized in a polymer film. The index of refraction of the polymer is high, so in their experiment, the glancing illumination traverses the polymer rather than generating an evanescent wave. Unpolarized images were recorded by video camera, making the method sensitive to absorption dipole only. They showed that five combinations of illumination paths and orientations are sufficient to fully determine the three-dimensional orientation, resolving all of the symmetry-related ambiguities (except that between (θ,ϕ) and $(180° - \theta,\phi - 180°)$, which is intrinsic to the fluorophore). Prummer et al.[50] point out, in agreement with our experience, that further illumination directions would add useful redundant information at the expense of time resolution.

Full detection of the three-dimensional orientation without ambiguities can provide important mechanistic information. In the example above, the motions of actin are obscured to some extent by the symmetry of the optical arrangement, and in a study of the unconventional myosin V,[20] quantitative estimation of the myosin angular stroke depended on assumptions about β vs $180° - \beta$.

Other Techniques

Nanosecond Time-Resolved Anisotropy. Several studies have reported nanosecond time-resolved polarization measurements on single molecules.[51,52] The most common arrangement is a spot-confocal microscope in which molecules of interest diffuse in and out of the detection volume, producing a burst of photons. With brief (nanosecond) pulsed excitation and appropriate resolution of the arrival time for photons detected through orthogonal polarizers, the decay of fluorescence anisotropy can be calculated. The anisotropy is usually defined by $r(t) = [I_{||}(t) - I_{\perp}(t)]/[I_{||}(t) + 2I_{\perp}(t)]$, where the subscripts refer to the polarization of the detector relative to that of the exciting light. Mixing of polarized emission between the two detector channels due to refraction by the objective lens must be taken into account.[33,51,53] As mentioned earlier, the initial anisotropy $r(0)$ relates to the collinearity of the absorption and emission dipole moments, distortions of the molecule, and rotational motions much faster than the instrument dead time. The subsequent time course of $r(t)$, usually a decay from $r(0)$ toward zero, gives a direct indication of rotational motion on the time scale of the fluorescence lifetime, τ_f, and severalfold longer. When the molecules are freely diffusing in solution, the average orientation distribution is isotropic, so no absolute angles are available. Nanosecond time-resolved anisotropy is also possible using immobilized molecules, but with the additional complexity over snapshot recording of average polarization, this method has not been widely adopted.

Orientation Sensitive Image Formation. The interaction between the absorption dipole and the polarization of the excitation field and the spatial distribution of light emitted from an individual dipole have been employed to form intensity distributions that carry the orientational information. Images of individual dipoles slightly away from the plane of focus, especially ones near a dielectric interface[54] and when spherical aberration is purposefully introduced into the collecting optics,[55−57] have side lobes and fringes due to the spatial distribution of polarized light near the focus of a high aperture objective. These features have been employed to determine the three-dimensional orientation of fluorescence emission dipoles and to characterize the dynamics of fluorophore motions in polymer films.[58]

Annular illumination from only the edges of a high aperture objective lens produces a strong *z*-axis component of polarization at the focal point and a spatial distribution of polarizations that can be scanned across the molecule to interrogate its orientation.[59,60] In Figure 7,[61] the upper three panels show theoretical distributions of total fluorescence intensity as the focal point of such an annular illumination spot is raster-scanned in the $x-y$ plane across a molecule. The exciting beam entering the back of the objective is polarized in the *x* direction. The three distributions are calculated for a dipole located at a polymer/air interface and polarized in the *x*, *y*, and *z* directions. The differences among the intensity patterns demonstrate the orientation sensitivity of this method. Sick et al.[60] provide very clear ray-optics explanations for the shapes of these expected distributions, due to peripheral rays that contain polarization vectors out of the $x-y$ plane that combine and interfere in spatially distinctive patterns. Experimental images of individual DiI molecules in a thin polymer film (Figure 7, lower panels) show very similar patterns. In general, the distribution of intensity is a combination of the three orthogonal patterns, which can be fitted to the actual measurements to estimate the polar angles in the microscope coordinate frame. The same symmetry-related ambiguities as discussed above for *x*-, *y*-, and *z*-oriented fluorescence polarization meth-

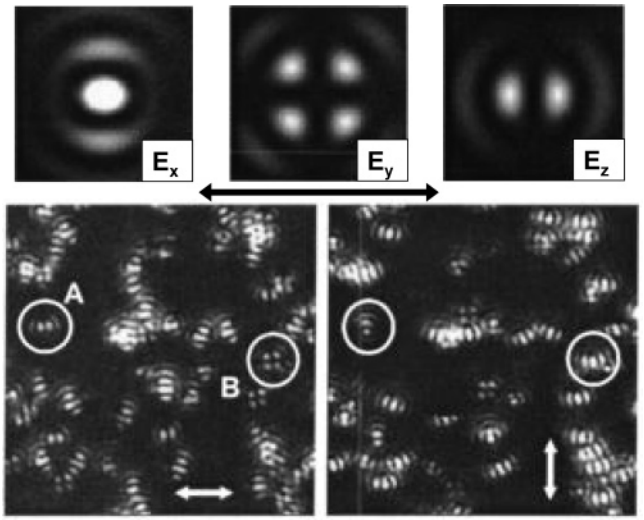

FIGURE 7. Determination of probe orientation with high numerical aperture annular illumination entering the objective with *x*-polarization (double-headed black arrow). Theoretical spatial distributions of unpolarized fluorescence intensity are calculated for a dipole located at a polymer/air interface and oriented in the *x*, *y*, and *z* directions (upper panels). Experimental images of individual DiI molecules in a thin polymer film (lower panels, *x*-polarization on the left, *y*-polarization on the right) show very similar patterns or combinations of the orthogonal patterns. Adapted from ref 61 with permission.

ods (θ vs $180° - \theta$ and ϕ vs $-\phi$) are present in this system. The angular precision is $\sim 5°$ at 1 s sampling time.[50,52]

Direct imaging of the spatial emission pattern in the back focal plane of the objective is shown in Figure 8.[29] The top panels give expected patterns of intensity for various dipole orientations, and experimental recordings are shown below. The experimental setup enabled illumination with *x*- or *y*-polarized light and also with radially polarized excitation. The radial polarization provides a strong *z*-axis illumination,[62] similar to annular excitation. The pairs of intensity distributions recorded with *x*- and *y*-polarization or else *x*- and radially polarized input beams are the same, indicating (as explained in regard to Figure 3) that the type of illumination does not alter the characteristics of radiation from the excited state of an immobilized single molecule. The bright ring of intensity at the periphery of each distribution comes from rays captured beyond the critical angle for total internal reflection. More optical power is contained in the outer ring than in the rest of the image, indicating that near-field light collection by the microscope slide surface is an important factor.

The precision of angular determination for midrange angles in the experiment of Figure 8 was 2° at a time resolution of 1 s. The performance could probably be improved using brighter illumination, faster acquisition by pixel binning, and collection of polarized images. Leib et al.[29] point out that with emission pattern imaging, problems such as blinking, optical aberrations in the microscope objective, and the exact axial and lateral location of the molecule all affect the results less than in methods that use imaging of the absorption dipole. Only

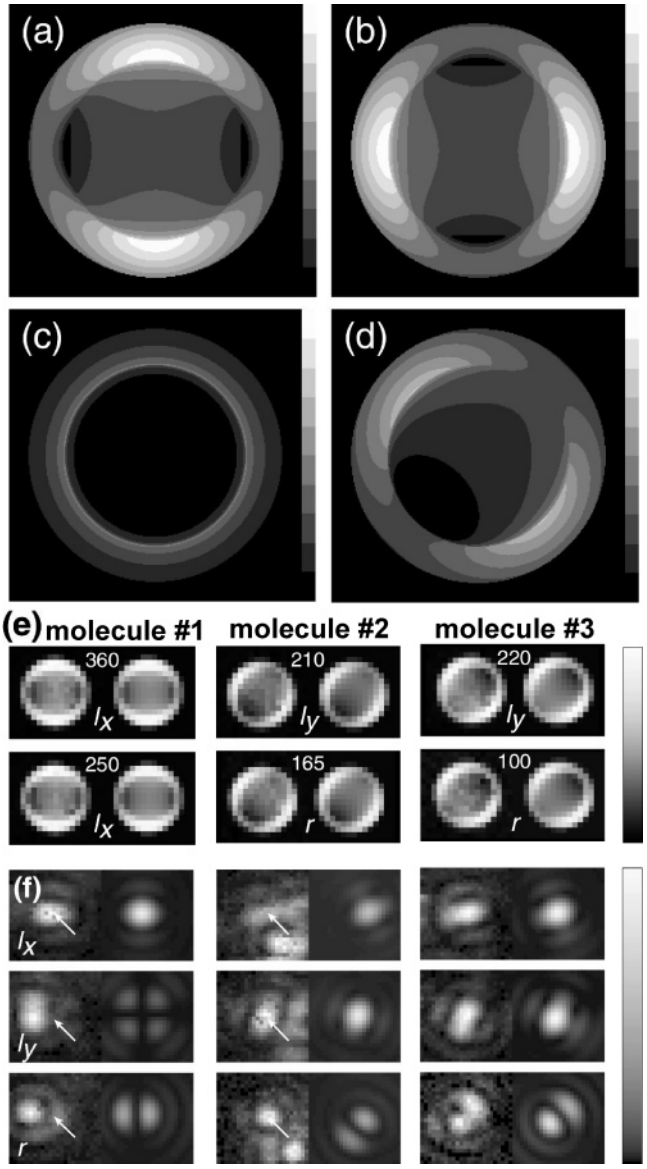

FIGURE 8. Imaging of the pattern of emission paths and the back focal plane of a collecting objective. Theoretical emission patterns of dipoles at an air-glass interface with orientations (θ and ϕ) (a) (90°,0°), (b) (90°,90°), (c) (0°,0°), and (d) (45°,45°). The outer ring of bright light is emission collected beyond the critical angle for total internal reflection. Note that the pattern in panel d is different from that expected for $(\theta,\phi) = (45°,135°)$, breaking a symmetry common to other techniques. Panel e shows experimental patterns of emission path for three selected molecules. The left-hand images are the measured data, and right-hand images are best fits. White numbers in the top centers are maximum intensities. I_x (I_y) denotes excitation with an *x*-polarized (*y*-polarized) Gaussian beam, and *r* denotes excitation with radial polarization. Note that the emission pattern does not depend on the polarization of the excitation. Panel f shows comparison of the spatial fluorescence emission distributions (similar to those in Figure 7) for the same three molecules (left-hand images) with patterns expected for dipole orientations determined from panel e (right-hand images). White arrows designate the molecule of interest if another molecule is nearby. Adapted from ref 29 with permission.

one molecule is interrogated at a time, similar to the fluorescence polarization technique discussed above with APD detectors, whereas imaging of the emission dipoles

can be done together by confocal scanning of several molecules (Figure 7). All of the methods in this section currently use algorithms that predict intensity distributions only for static molecules. Therefore motions of the molecule during the recording time must be minimal. By contrast, as explained above, SMFP intrinsically detects motions together with the average orientation. These various techniques complement each other well.

Conclusions

Applications of single molecule fluorescence polarization and orientation-sensitive imaging of absorption and emission dipoles to mechanistic questions in macromolecular biophysics are emerging. A number of incarnations trade off complexity against time resolution, angular resolution, and removal of angular ambiguities. Future developments will provide improved temporal and angular resolution and combine angular detection with other compatible methodologies, such as infrared optical traps, atomic force microscopy, and nanometer-scale resolution of spatial position. Orientation-sensitive single-molecule spectroscopy has been combined with other dynamic signals to simultaneously record extensive spectral fingerprints of single molecules.[51,52,63] As many cellular protein and nucleic acid machines use rotational motions as crucial features of their functional output, the techniques to detect these motions are important elements in the single-molecule biophysicist's toolkit.

This work was supported by NIH Research Grants AR26846, AR51174, and GM63205. The acetamidotetramethyl rhodamine was a generous gift from Dr. John E.T. Corrie, NIMR, Mill Hill, London. We thank Ms. Mojdeh Toomarian for useful comments.

References

(1) Mannuzzu, L. M.; Moronne, M. M.; Isacoff, E. Y. Direct Physical Measure of Conformational Rearrangement Underlying Potassium Channel Gating. *Science* **1996**, *271*, 213−216.
(2) Dominguez, R.; Freyzon, Y.; Trybus, K. M.; Cohen, C. Crystal Structure of a Vertebrate Smooth Muscle Myosin Motor Domain and its Complex with the Essential Light Chain: Visualization of the Pre-Power Stroke State. *Cell* **1998**, *94*, 559−571.
(3) Yasuda, R.; Noji, H.; Kinosita, K., Jr.; Yoshida, M. F_1-ATPase Is a Highly Efficient Molecular Motor that Rotates with Discrete 120° Steps. *Cell* **1998**, *93*, 1117−1124.
(4) Zhang, Z.; Huang, L.; Shulmeister, V. M.; Chi, Y.-I.; Kim, K. K.; Hung, L.-W.; Crofts, A. R.; Berry, E. A.; Kim, S.-H. Electron Transfer by Domain Movement in Cytochrome bc_1. *Nature* **1998**, *392*, 677−684.
(5) Clark, B. F. C.; Thirup, S.; Kjeldgaard, M.; Nyborg, J. Structural Information for Explaining the Molecular Mechanism of Protein Biosynthesis. *FEBS Lett.* **1999**, *452*, 41−46.
(6) Jiang, Y.; Lee, A.; Chen, J.; Ruta, V.; Cadene, M.; Chait, B. T.; MacKinnon, R. X-ray Structure of a Voltage-Dependent K^+ Channel. *Nature* **2003**, *423*, 33−41.
(7) Goldman, Y. E. Wag the Tail: Structural Dynamics of Actomyosin. *Cell* **1998**, *93*, 1−4.
(8) Geeves, M. A.; Holmes, K. C. Structural Mechanism of Muscle Contraction. *Annu. Rev. Biochem.* **1999**, *68*, 687−728.
(9) Rice, S.; Lin, A. W.; Safer, D.; Hart, C. L.; Naber, N.; Carragher, B. O.; Cain, S. M.; Pechatnikova, E.; Wilson-Kubalek, E. M.; Whittaker, M.; Pate, E.; Cooke, R.; Taylor, E. W.; Milligan, R. A.; Vale, R. D. A Structural Change in the Kinesin Motor Protein that Drives Motility. *Nature* **1999**, *402*, 778−784.
(10) Rayment, I.; Holden, H. M.; Whittaker, M.; Yohn, C. B.; Lorenz, M.; Holmes, K. C.; Milligan, R. A. Structure of the Actin-Myosin Complex and Its Implications for Muscle Contraction. *Science* **1993**, *261*, 58−65.
(11) Cooke, R.; Crowder, M. S.; Thomas, D. D. Orientation of Spin Labels Attached to Cross-Bridges in Contracting Muscle Fibres. *Nature* **1982**, *300*, 776−778.
(12) Irving, M.; Allen, T. S. C.; Sabido-David, C.; Craik, J. S.; Brandmeier, B.; Kendrick-Jones, J.; Corrie, J. E. T.; Trentham, D. R.; Goldman, Y. E. Tilting of the Light-Chain Region of Myosin During Step Length Changes and Active Force Generation in Skeletal Muscle. *Nature* **1995**, *375*, 688−691.
(13) Forkey, J. N.; Quinlan, M. E.; Goldman, Y. E. Protein Structural Dynamics by Single-Molecule Fluorescence Polarization. *Prog. Biophys. Mol. Biol.* **2000**, *74*, 1−35.
(14) Ha, T.; Enderle, Th.; Chemla, D. S. Single Molecule Dynamics Studied by Polarization Modulation. *Phys. Rev. Lett.* **1996**, *77*, 3979−3982.
(15) Ha, T.; Glass, J.; Enderle, Th.; Chemla, D. S.; Weiss, S. Hindered Rotational Diffusion and Rotational Jumps of Single Molecules. *Phys. Rev. Lett.* **1998**, *80*, 2093−2096.
(16) Zhaung, X.; Bartley, L. E.; Babcock, H. P.; Russell, R.; Ha, T.; Herschlag, D.; Chu, S. A Single-Molecule Study of RNA Catalysis and Folding. *Science* **2000**, *288*, 2048−2051.
(17) Nishizaka, T.; Oiwa, K.; Noji, H.; Kimura, S.; Muneyuki, E.; Yoshida, M.; Kinosita, K., Jr. Chemomechanical Coupling in F_1-ATPase Revealed by Simultaneous Observation of Nucleotide Kinetics and Rotation. *Nat. Struct. Mol. Biol.* **2004**, *11*, 142−148.
(18) Sase, I.; Miyata, H.; Ishiwata, S.; Kinosita, K., Jr. Axial Rotation of Sliding Actin Filaments Revealed by Single-Fluorophore Imaging. *Proc. Natl. Acad. Sci. U.S.A.* **1997**, *94*, 5646−5650.
(19) Warshaw, D. M.; Hayes, E.; Gaffney, D.; Lauzon, A.-M.; Wu, J.; Kennedy, G.; Trybus, K.; Lowey, S.; Berger, C. Myosin Conformational States Determined by Single Fluorophore Polarization. *Proc. Natl. Acad. Sci. U.S.A.* **1998**, *95*, 8034−8039.
(20) Forkey, J. N.; Quinlan, M. E.; Shaw, M. A.; Corrie, J. E. T.; Goldman, Y. E. Three-Dimensional Structural Dynamics of Myosin V by Single-Molecule Fluorescence Polariztion. *Nature* **2003**, *422*, 399−404.
(21) Sosa, H.; Peterman, E. J. G.; Moerner, W. E.; Goldstein, L. S. B. ADP−Induced Rocking of the Kinesin Motor Domain Revealed by Singe-Molecule Fluorescence Polarization Microscopy. *Nat. Struct. Biol.* **2001**, *8*, 540−544.
(22) Asenjo, A. B.; Krohn, N.; Sosa, H. Configuration of the Two Kinesin Motor Domains During ATP Hydrolysis. *Nat. Struct. Biol.* **2003**, *10*, 836−842.
(23) Corrie, J. E. T.; Brandmeier, B. D.; Ferguson, R. E.; Trentham, D. R.; Kendrick-Jones, J.; Hopkins, S. C.; van der Heide, U. A.; Goldman, Y. E.; Sabido-David, C.; Dale, R. E.; Criddle, S.; Irving, M. Dynamic Measurement of Myosin Light-Chain-Domain Tilt and Twist in Muscle Contraction. *Nature* **1999**, *400*, 425−430.
(24) Ferguson, R. E.; Sun, Y.-B.; Mercier, P.; Brack, A. S.; Sykes, B. D.; Corrie, J. E. T.; Trentham, D. R.; Irving, M. In Situ Orientations of Protein Domains: Troponin C in Skeletal Muscle Fibers. *Mol. Cell* **2003**, *11*, 865−874.
(25) Sale, K.; Sar, C.; Sharp, K. A.; Hideg, K.; Fajer, P. G. Structural Determination of Spin Label Immobilization and Orientation: A Monte Carlo Minimization Approach. *J. Magn. Reson.* **2002**, *156*, 104−112.
(26) Ha, T.; Laurence, T. A.; Chemla, D. S.; Weiss, S. Polarization Spectroscopy of Single Fluorescent Molecules. *J. Phys. Chem. B* **1999**, *103*, 6839−6850.
(27) Peterman, E. J. G.; Sosa, H.; Moerner, W. E. Single-Molecule Fluorescence Spectroscopy and Microscopy of Biomolecular Motors. *Annu. Rev. Phys. Chem.* **2004**, *55*, 79−96.
(28) Lakowicz, J. R. *Principles of Fluorescence Spectroscopy*, 2nd ed.; Plenum Publishers: New York, 1999; pp 291−319.
(29) Lieb, M. A.; Zavislan, J. M.; Novotny, L. Single-Molecule Orientations Determined by Direct Emission Pattern Imaging. *J. Opt. Soc. Am. B* **2004**, *21*, 1210−1215.
(30) Adachi, K.; Yasuda, R.; Noji, H.; Itoh, H.; Harada, Y.; Yoshida, M.; Kinosita, K., Jr. Stepping Rotation of F_1-ATPase Visualized Through Angle-Resolved Single-Fluorophore Imaging. *Proc. Natl. Acad. Sci. U.S.A.* **2000**, *97*, 7243−7247.
(31) Forkey, J. N.; Quinlan, M. E.; Goldman, Y. E. Measurement of Single Macromolecules Orientation by Total Internal Reflection Fluorescence Polarization Microscopy. *Biophys. J.*, submitted for publication, 2004.
(32) Axelrod, D.; Burghardt, T. P.; Thompson, N. L. Total Internal Reflection Fluorscence. *Annu. Rev. Biophys. Bioeng.* **1984**, *13*, 247−268.
(33) Axelrod, D. Fluorescence Polarization Microscopy. *Methods Cell Biol.* **1989**, *30*, 333−352.
(34) Chen, R. F.; Bowman, R. L. Fluorescence Polarization: Measurement with Ultraviolet-Polarizing Filters in a Spectrophotofluorometer. *Science* **1965**, *147*, 729−732.

(35) Penzkofer, A.; Wiedmann, J. Orientation of Transition Dipole Moments of Rhodamine 6G Determined by Excited State Absorption. *Opt. Commun.* **1980**, *35*, 81−86.
(36) Dale, R. E.; Hopkins, S. C.; van der Heide, U. A.; Marszalek, T.; Irving, M.; Goldman, Y. E. Model-Independent Analysis of the Orientation of Fluorescent Probes with Restricted Mobility in Muscle Fibers. *Biophys. J.* **1999**, *76*, 1606−1618.
(37) Cantor, C. R.; Schimmel, P. R. *Biophysical Chemistry*; W. H. Freeman Co.: New York, 1980; Part II, pp 433−480.
(38) Ambrose, W. P.; Goodwin, P. M.; Martin, J. C.; Keller, R. A. Single Molecule Detection and Photochemistry on a Surface Using Near-Field Optical Excitation. *Phys. Rev. Lett.* **1994**, *72*, 160−163.
(39) Xie, X. S.; Dunn, R. C. Probing Single Molecule Dynamics. *Science* **1994**, *265*, 361−364.
(40) Quinlan, M. E.; Forkey, J. N.; Goldman, Y. E. Orientation of the Myosin Light Chain Region by Single and Multiple Molecule Total Internal Reflection Fluorescence Polarization Microscopy. *Biophys. J.*, submitted for publication, 2004.
(41) Dickson, R. M.; Cubitt, A. B.; Tsien, R. Y.; Moerner, W. E. On/Off Blinking and Switching Behaviour of Single Molecules of Green Fluoresent Protein. *Nature* **1997**, *388*, 355−358.
(42) Pierce, D. W.; Hom-Booher, N.; Vale, R. D. Imaging Individual Green Fluorescent Proteins. *Nature* **1997**, *388*, 338.
(43) Bopp, M. A.; Jia, Y.; Li, L.; Cogdell, R. J.; Hochstrasser, R. M. Fluorescence and Photobleaching Dynamics of Single Light-Harvesting Complexes. *Proc. Natl. Acad. Sci. U.S.A.* **1997**, *94*, 10630−10635.
(44) Vanden Bout, D. A.; Yip, W.-T.; Hu, D.; Fu, D.-K.; Swager, T. M.; Barbara, P. F. Discrete Intensity Jumps and Intramolecular Electronic Energy Transfer in the Spectroscopy of Single Conjugated Polymer Molecules. *Science* **1997**, *277*, 1074−1077.
(45) Gordon, M. P.; Ha, T.; Selvin, P. R. Single-Molecule High-Resolution Imaging With Photobleaching. *Proc. Natl. Acad. Sci. U.S.A.* **2004**, *101*, 6462−6465.
(46) Nishizaka, T.; Yagi, T.; Tanaka, Y.; Ishiwata, S. Right-Handed Rotation of an Actin Filament in an *in Vitro* Motile System. *Nature* **1993**, *361*, 269−271.
(47) Ali, M. Y.; Uemura, S.; Adachi, K.; Itoh, H.; Kinosita, K., Jr.; Ishiwata, S. Myosin V is a Left-Handed Sprial Motor on the Right-Handed Actin Helix. *Nat. Struct. Biol.* **2002**, *9*, 464−467.
(48) Suzuki, N.; Miyata, H.; Ishiwata, S.; Kinosita, K., Jr. Preparation of Bead-Tailed Actin Filaments: Estimation of the Torque Produced by the Sliding Force in an in Vitro Motility Assay. *Biophys. J.* **1996**, *70*, 401−408.
(49) Ali, M. Y.; Homma, K.; Iwane, A. H.; Adachi, K.; Itoh, H.; Kinosita, K., Jr.; Yanagida, T.; Ikebe, M. Unconstrained Steps of Myosin VI Appear Longest among Known Molecular Motors. *Biophys. J.* **2004**, *86*, 3804−3810.
(50) Prummer, M.; Sick, B.; Hecht, B.; Wild, U. P. Three-Dimensional Optical Polarization Tomography of Single Molecules. *J. Chem. Phys.* **2003**, *118*, 9824−9829.
(51) Schaffer, J.; Volkmer, A.; Eggeling, C.; Subramaniam, V.; Striker, G.; Seidel, C. A. M. Identification of Single Molecules in Aqueous Solution by Time-Resolved Fluorescence Anisotropy. *J. Phys. Chem. A* **1999**, *103*, 331−336.
(52) Prummer, M.; Sick, B.; Renn, A.; Wild, U. P. Multiparameter Microscopy and Spectroscopy for Single-Molecule Analytics. *Anal. Chem.* **2004**, *76*, 1633−1640.
(53) Koshioka, M.; Sasaki, K.; Masuhara, H. Time-Dependent Fluorescence Depolarization Analysis in Three-Dimensional Microspectroscopy. *Appl. Spectrosc.* **2004**, *49*, 224−228.
(54) Böhmer, M.; Enderlein, J. Orientation Imaging of Single Molecules by Wide-Field Epifluorescence Microscopy. *J. Opt. Soc. Am. B* **2003**, *20*, 554−559.
(55) Dickson, R. M.; Norris, D. J.; Moerner, W. E. Simultaneous Imaging of Individual Molecules Aligned Both Parallel and Perpendicular to the Optic Axis. *Phys. Review. Lett.* **1998**, *81*, 5322−5325.
(56) Bartko, A. P.; Dickson, R. M. Imaging Three-Dimensional Single Molecule Orientations. *J. Phys. Chem. B* **1999**, *103*, 11237−11241.
(57) Bartko, A. P.; Dickson, R. M. Three-Dimensional Orientations of Polymer-Bound Single Molecules. *J. Phys. Chem. B* **1999**, *103*, 3053−3056.
(58) Bartko, A. P.; Xu, K.; Dickson, R. M. Three-Dimensional Single Molecule Rotational Diffusion in Glassy State Polymer Films. *Phys. Rev. Lett.* **2002**, *89*, 026101-1−026101-4.
(59) Sick, B.; Hecht, B.; Novotny, L. Orientational Imaging of Single Molecules by Annular Illumination. *Phys. Rev. Lett.* **2000**, *85*, 4482−4485.
(60) Sick, B.; Hecht, B.; Wild, U. P.; Novotny, L. Probing Confined Fields With Single Molecules and *Vice Versa*. *J. Microsc.* **2001**, *202*, 365−373.
(61) Kreiter, M.; Prummer, M.; Hecht, B.; Wild, U. P. Orientation Dependence of Fluorescence Lifetimes Near an Interface. *J. Chem. Phys.* **2002**, *117*, 9430−9433.
(62) Novotny, L.; Beversluis, M. R.; Youngworth, K. S.; Brown, T. G. Longitudinal Field Modes Probed by Single Molecules. *Phys. Rev. Lett.* **2001**, *86*, 5251−5254.
(63) Cognet, L.; Harms, G. S.; Blab, G. A.; Lommerse, P. H. M.; Schmidt, T. Simultaneous Dual-Color and Dual-Polarization Imaging of Single Molecules. *Appl. Phys. Lett.* **2000**, *77*, 4052−4054.

AR040137K